ELSEVIER

Infrared Physics & Technology 44 (2003) 79–84

INFRARED PHYSICS & TECHNOLOGY

www.elsevier.com/locate/infrared

High field p-Ge laser operation in permanent magnet assembly

C.J. Fredricksen [a], E.W. Nelson [b], A.V. Muravjov [b], R.E. Peale [b,*]

[a] *Zaubertek, Inc., 12565 Research Parkway Suite 300, Orlando, FL 32826, USA*
[b] *Department of Physics, University of Central Florida, Orlando, FL 32816, USA*

Received 7 May 2002

Abstract

Operation of the far-infrared gallium-doped p-type germanium laser in the broadband range above 70 cm^{-1}, which requires relatively high magnetic fields, is demonstrated using novel permanent magnet assemblies. NdFeB and SmCo magnet assemblies were compared. The applied field from a NdFeB assembly was found to decrease strongly on cooling to the cryogenic temperature required for p-Ge laser operation, but that of a SmCo assembly changes insignificantly.

PACS: 42.55.Px; 42.60.By; 42.72.Ai; 75.50.Ww

Keywords: Far infrared; Terahertz; Laser; p-Ge; Germanium; SmCo; NdFeB; Permanent magnet

1. Introduction

The p-Ge laser is a solid-state laser operating in the 1.5–4.2 THz region of the electromagnetic spectrum [1]. Features include wide tunability [2,3], watt-level power concentrated in a single axial mode [4] of MHz width [5], and picosecond pulse generation [6,7]. It has numerous potential applications, which include chemical sensing, communications, and non-destructive testing. A practical challenge is the operational requirement for the active crystal to be placed in a uniform and fairly strong magnetic field at cryogenic temperatures [1].

The laser mechanism is based on intersubband transitions of hot holes. The inversion population arises in applied crossed electric and magnetic fields. The laser emission spectrum depends on applied magnetic field. At low fields, from 0.3 to 0.75 T, the laser generates a few narrow lines at wave numbers below 60 cm^{-1} associated with intracenter transitions of shallow acceptors (e.g. Ga). At higher fields, in the range 0.5–2 T, the laser has broadband gain, with a typical spectral width of up to 30 cm^{-1}, which can be tuned from 70 to 140 cm^{-1} by increasing the magnetic field. Fig. 1 shows typical operation zones for a Ga-doped germanium active crystal.

Traditional p-Ge lasers have the active crystal installed within a superconducting solenoid immersed in liquid helium. However, recent reports [8] prove that the p-Ge laser can operate in closed cycle refrigerators. Although superconducting

* Corresponding author. Tel.: +1-407-823-5208; fax: +1-407-823-5112.
E-mail address: rep@physics.ucf.edu (R.E. Peale).

1350-4495/02/$ - see front matter
PII: S1350-4495(02)00179-2

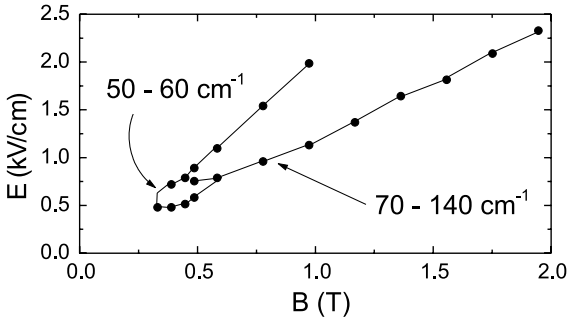

Fig. 1. Characteristic generation zones in the space of applied electric (E) and magnetic (B) fields for a far-infrared p-Ge laser based on Ga-doped material. Two regions of laser operation are indicated with their range of emission frequencies. The high field region is the most advantageous for spectroscopic applications.

solenoids in principle can operate in closed cycle refrigerators, all demonstrations to date used assemblies of permanent magnets to apply the necessary field. Advantages are compactness and absence of current leads, which thermally load the cooler.

This paper reports p-Ge laser operation using novel permanent magnet assemblies based on NdFeB or SmCo magnets. So far, all reported p-Ge lasers in permanent magnet assemblies used only NdFeB magnets. Applied fields measured at room temperature were 0.35 T [9], 0.42 T [8], and 0.7 T [10]. Actual applied fields at cryogenic temperatures are likely to have been significantly lower, as suggested by results presented here. In [9] use of Ga-doped Ge crystal and relatively weak applied magnetic field caused the laser to operate only in the low-field zone (Fig. 1), where the emission spectrum is affected by Ga impurity intracenter transitions. In [8], this was overcome by using Be deep-acceptor doped Ge [11], where the acceptor absorption lines are outside the laser emission spectrum and laser works in broad-band-gain mode even at such low magnetic field. In [10], planar film geometry allowed close-spacing of the NdFeB magnets to obtain higher fields applied to a Ge:Be active layer.

Ge:Ga material has advantages of lower cost and higher availability compared with Ge:Be, but applied fields must be high enough to exploit the broad gain spectrum of the high-field zone (Fig. 1). Large active-crystals are attractive for potential applications such as laser remote sensing, laser free-space communications, and non-destructive testing, which need high output intensities and optimal beam quality. However, large crystals require large air gaps in the magnetic assembly, which works against high field strength and uniformity. To apply high magnetic fields to large active Ge:Ga crystals, innovative magnet assemblies are required. This paper reports successful use of new magnet assemblies that allow high field operation of Ge:Ga active crystals having traditional $\sim$1 cm^3 volume. A modified NdFeB assembly, based on [9], and a novel SmCo assembly were tested and compared.

2. Experimental

Fig. 2 shows cross sections of four permanent magnet assemblies studied in this work. The first three (Fig. 2A–C) employ NdFeB bar magnets (dark shading, Magnet Sales #35, BH = 35 kOe kG) with soft iron yokes and poles. The

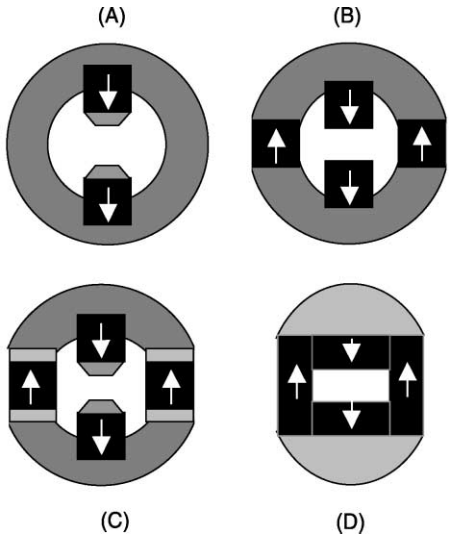

Fig. 2. Schematic cross sections of permanent magnet assemblies. A, B, and C employ NdFeB magnets (dark squares) and soft iron yokes and pole pieces (light shading). Assembly D employs SmCo magnets and stainless steel yoke. Arrows indicate magnetization direction.

spacers in Fig. 2C were cut from sheet steel. Fig. 2D shows a novel magnet assembly designed and constructed by Magnet Sales for our experiments. The bar magnets (dark shading) are SmCo and the yokes are magnetic stainless steel. Arrows give magnetization directions.

All experiments were performed using the Eagle-Picher Ge:Ga material used in [9]. The laser rod used with the NdFeB magnet assembly had dimensions 38 mm × 7.7 mm × 3.8 mm with orientations $[1\,1\,0] \times [1\,-1\,0] \times [0\,0\,1]$, respectively. This crystal was polished on all surfaces such that it operated on total internal reflection modes. Ohmic contacts (GaIn alloy) were soldered on the narrow lateral faces, so that high voltage could be applied in the [1 −1 0] direction. The laser emission was detected in the direction of the long axis [1 1 0], and the magnetic field was applied along the transverse [0 0 1] direction (Voigt configuration).

The laser rod used with the SmCo magnet assembly was the same as used in [9], except that the dimension in the direction of the magnetic field had been reduced. The final dimensions were 51 mm × 4.1 mm × 3.7 mm with orientations $[1\,1\,0] \times [1\,-1\,0] \times [0\,0\,1]$. Ohmic contacts (indium) were soldered to the 51 mm × 3.7 mm faces, so that field orientations were the same as for the first crystal. $SrTiO_3$ mirrors were attached to polished ends of the active crystal, forming an axial mode Fabry–Perot resonator. All lateral surfaces of the active crystal were rough ground to prevent laser operation on total reflection modes.

Each permanent magnet assembly was attached to an insert for a liquid helium dewar. High voltage electric field pulses of μs duration were applied to the laser rods from a thyratron pulser. Radiation was detected by a Ge:Ga photoconducting detector in the same dewar.

Permanent magnet experiments were compared with results for the 51 mm crystal in the Voigt-configured field of a room-temperature electromagnet (Walker). Here, the crystal was mounted at the end of a 13 mm diameter brass light pipe, which was inserted into a liquid-helium cryostat. The tail stock of the cryostat was placed between the 9 in.-diameter pole faces of the magnet. Radiation was detected at the light-pipe output using a 4 K Si composite bolometer (Infrared Labs).

Strength and uniformity of the room-temperature magnetic flux density B in the air gap between poles of the permanent magnet assemblies were measured using a Hall probe (F.W. Bell) mounted on a micrometer controlled translation stage. The temperature dependence of the magnetic field for SmCo and NdFeB was determined using a closed cycle refrigerator (CTI). Magnet samples were thermally anchored to a copper cold finger. The cold-finger temperature was monitored by a mechanically attached silicon-diode thermometer. The magnetic field, typically several tens of Gauss, was measured outside the vacuum jacket of the cooler using the Hall probe while cooling the magnet to 8 K.

3. Results

Fig. 3 shows calculated field lines for the Fig. 2B and D magnets performed using commercial finite element analysis software (FlexPDE). Measured field values are about 10% smaller than the calculated values. The difference arises from uncertainty in the magnetization value used in the calculation. We noticed that the field measured at the surface of different NdFeB samples from the same batch had different values and that these variations seemed to become more severe after thermal cycling. Note that the SmCo (Fig. 2D) design has a larger region of uniform field, making it easier to apply uniform magnetic field to the entire active crystal volume.

Fig. 4 shows the magnetic field measured at room temperature as a function of position near one end of each magnet assembly shown in Fig. 2. Without poles, the NdFeB magnetic field uniformity is poor. Without bevels, iron poles decrease the field strength in the air gap. Beveled poles concentrate the field to give higher values. The field of the pole-less SmCo magnet is quite strong and uniform.

Fig. 5 shows the temperature dependence of the magnetic field from NdFeB and SmCo magnets. The data were scaled so that the room temperature values match those in the air gap of the corresponding room temperature assemblies (Fig. 4c and d). A decrease of a few percent is observed for

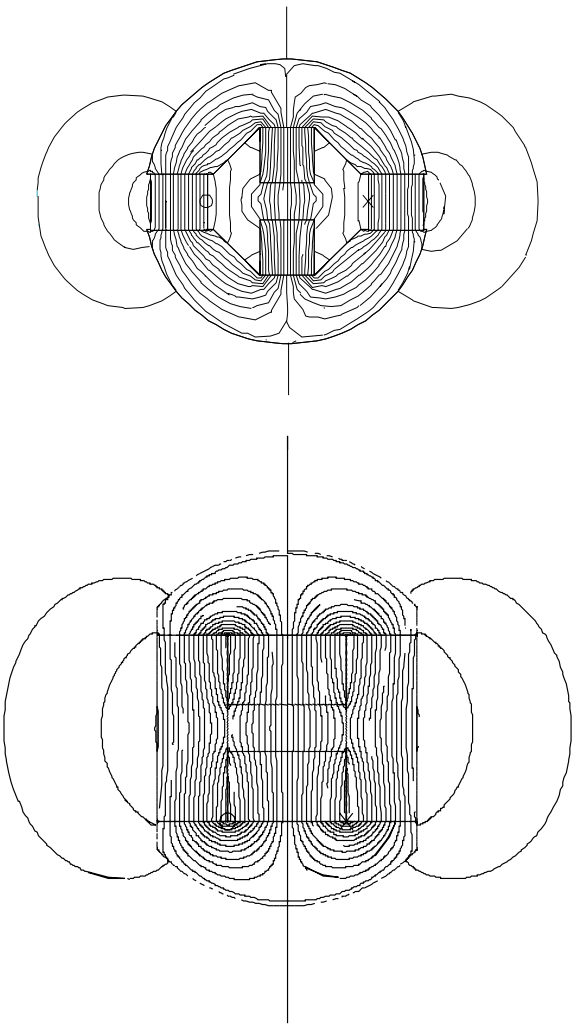

Fig. 3. Magnetic field lines for permanent magnet assemblies of Fig. 2B and D. The diameter of each magnet is 38 mm.

the SmCo magnet, with more rapid decrease at the lowest temperatures. In contrast, NdFeB shows first a slight increase and then a strong decrease of up to 25% starting already at 100 K.

Fig. 6 presents laser intensity vs. applied electric field for experiments performed with NdFeB and SmCo magnet assemblies (Fig. 2C and D, respectively). The room temperature magnetic fields in the air gaps of these assemblies (Fig. 4c and d) were 0.7 and 0.68 T, respectively. The SmCo assembly gives a broader generation zone, which occurs at higher applied electric fields.

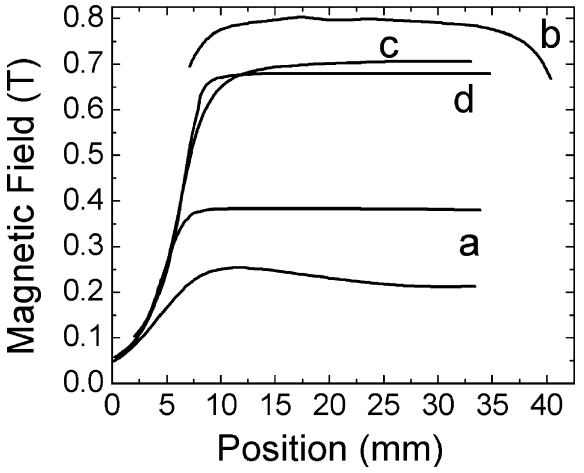

Fig. 4. Field strength and uniformity in air-gap of permanent magnet assemblies. The field is measured near one end, which is located for each assembly at $x = 7.5$ mm. Curves b, c, and d correspond to the assemblies shown in Fig. 2B, C, and D, respectively. The upper (lower) of curves a corresponds to the Fig. 2A assembly with (without) its iron pole pieces.

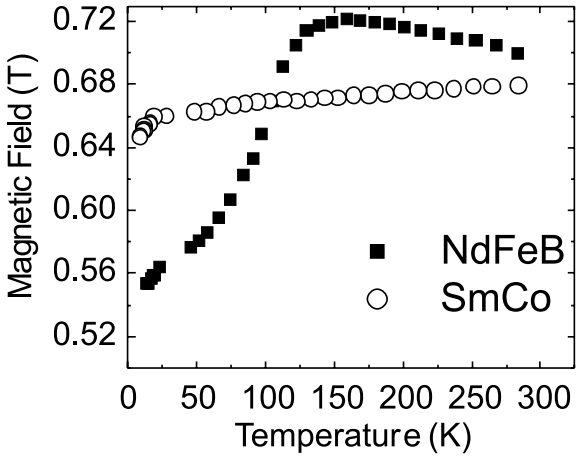

Fig. 5. Temperature dependence of the magnetic field for NdFeB (solid square symbols) and SmCo (open circle symbols) permanent magnet material. Each curve is separately scaled so that the room temperature value matches the air-gap field of the corresponding magnet assembly (Fig. 4b and c).

Fig. 7 shows the laser generation data for the 51 mm laser rod in the Voigt-configured room-temperature electromagnet. The open symbols indicate (E, B) points where emission was recorded. The thick diagonal lines indicate theoret-

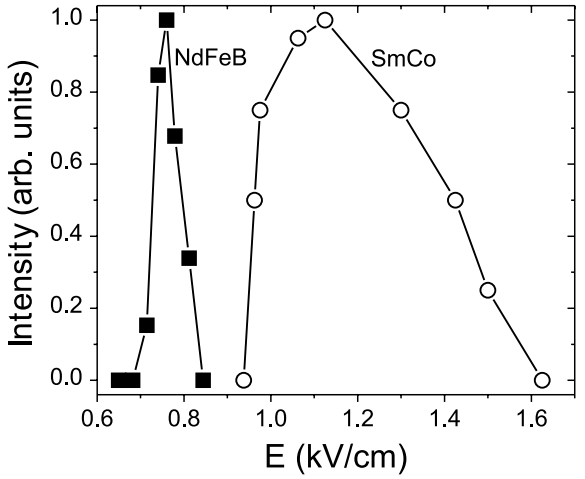

Fig. 6. Normalized laser intensity vs. applied electric field using NdFeB (Fig. 2C) and SmCo (Fig. 2D) permanent magnet assemblies.

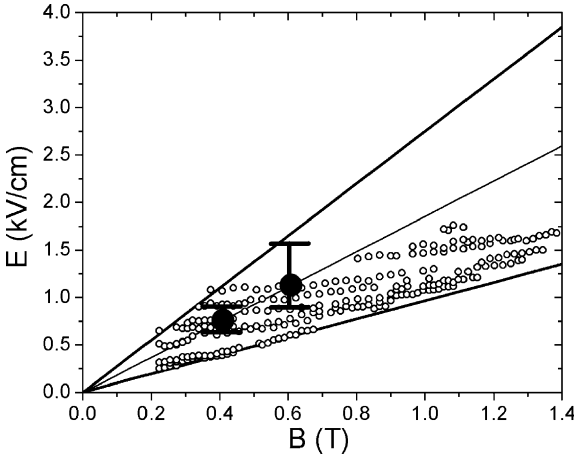

Fig. 7. Laser generation zone using electromagnet in Voigt configuration. The thick lines are theoretical E/B boundaries for the p-Ge laser mechanism. Observed laser generation points are represented as open circle symbols. The large solid circle symbols are placed on the bisector of the zone at the applied electric-field values corresponding to the emission maxima of Fig. 6. The solid bars through the open symbols give the lasing ranges of Fig. 6.

ical boundaries for p-Ge laser generation [12]. The large solid symbols are located at applied electric field values that correspond to maximum emission in Fig. 6. The vertical bars through these points indicate the range of laser generation recorded for each assembly in Fig. 6. The solid symbols are placed on the bisector (thin line) of the theoretical generation zone, which then determines the corresponding magnetic field applied by the permanent magnet assemblies at 4 K. Applied magnetic fields of ~0.4 and ~0.6 T are determined for the NdFeB and SmCo assemblies, respectively.

4. Discussion and conclusions

Operation of the p-Ge laser in the "high-field region" for an active Ga-doped germanium laser rod of traditional ~1 cm^3 volume has been obtained using NdFeB and SmCo permanent magnet assemblies. Room temperature measurements of the magnetic field uniformity show that the assemblies based on NdFeB magnets require iron pole pieces to provide adequate field homogeneity over the active crystal volume. The assembly based on SmCo provides adequate field uniformity without poles.

A strong loss of magnetization on cooling of the NdFeB magnet material (Fig. 5) is found. The effect for SmCo is comparatively weak. This means that SmCo is the better material for obtaining high fields at low temperature, even though NdFeB remanence (up to 1.4 T) is usually higher than for SmCo (up to 1.1 T).

A strong decrease in magnetic field applied to the active p-Ge crystal by the NdFeB assembly on cooling to 4 K is supported by Fig. 6, where the peak laser emission occurs at much lower applied electric field than for the SmCo assembly. The ratio E/B should be roughly constant for peak laser emission, which generally occurs near the center of the generation zone (Fig. 1). If the applied magnetic fields from the two assemblies were similar at 4 K, as they are at 300 K, the two generation curves in Fig. 6 would overlie each other more closely. Another point from Fig. 6 in favor of the SmCo assembly is the comparatively broad electric field range, which is direct evidence of stronger gain and better laser operation.

The applied magnetic field values from Fig. 7 of ~0.4 and ~0.6 T at 4 K for NdFeB and SmCo assemblies, respectively, are consistent with the temperature dependence reported in Fig. 5. In

summary, the data presented in Figs. 5–7 support a strong decrease with cooling in the applied magnetic field from the NdFeB assembly. The change for the SmCo assembly is comparatively small. In conclusion, the results presented in this paper demonstrate the advantages of using permanent magnet assemblies based on SmCo, rather than NdFeB, for high-field laser generation from active Ga-doped p-type germanium.

Acknowledgements

This work was supported by NSF (ECS-0070228) and by an AFOSR STTR phase II award (F49620-02-C-0027). Co-author from IPM thanks INTAS for partial support of this work (grant no. 97-0856).

References

[1] E. Gornik, A.A. Andronov (Eds.), Optical Quantum Electron., Special Issue on Far-infrared Semiconductor Lasers, 23, Chapman and Hall, London, 1991.
[2] S. Komiyama, H. Morita, I. Hosako, Continuous wavelength tuning of inter-valence-band laser oscillation in p-type Germanium over range of 80–120 μm, Jpn. J. Appl. Phys., Part 1 32 (1993) 4987–4991.
[3] A.V. Murav'ev, I.M. Nefedov, S.G. Pavlov, V.N. Shastin, Tunable narrowband laser that operates on interband transitions of hot holes in germanium, J. Sov. Quantum Electron. 23 (1993) 119–124.
[4] A.V. Muravjov, S.H. Withers, H. Weidner, R.C. Strijbos, S.G. Pavlov, V.N. Shastin, R.E. Peale, Single axial-mode selection in a far-infrared p-Ge laser, Appl. Phys. Lett. 76 (2000) 1996–1998.
[5] E. Bründermann, H.P. Röser, A.V. Muravjov, S.G. Pavlov, V.N. Shastin, Mode fine structure of the p-Ge intervalenceband laser measured by heterodyne mixing spectroscopy with an optically pumped ring gas laser, Infrared Phys. Technol. 36 (1995) 59.
[6] J.N. Hovenier, A.V. Muravjov, S.G. Pavlov, V.N. Shastin, R.C. Strijbos, W.Th. Wenckebach, Active mode locking of a p-Ge hot hole laser, Appl. Phys. Lett. 71 (1997) 443–445.
[7] A.V. Muravjov, S.H. Withers, R.C. Strijbos, S.G. Pavlov, V.N. Shastin, R.E. Peale, Actively mode-locked p-Ge laser in Faraday configuration, Appl. Phys. Lett. 75 (1999) 2882–2884.
[8] E. Brüderman, H.P. Röser, First operation of a far-infrared p-germanium laser in a standard closed-cycle machine at 15 K, Infrared Phys. Technol. 38 (1997) 201.
[9] K. Park, R.E. Peale, H. Weidner, J.J. Kim, Submillimeter p-Ge laser using a Voigt-configured permanent magnet, IEEE J. Quantum Electron. 32 (1996) 1203–1210.
[10] D.R. Chamberlin, E. Bründermann, E.E. Haller, Planar contact geometry for far-infrared germanium lasers, Appl. Phys. Lett. 74 (1999) 3761.
[11] E. Bründermann, A.M. Linhart, L. Reichertz, H.P. Röser, O.D. Dubon, W.L. Hansen, G. Sirmain, E.E. Haller, Double acceptor doped Ge: a new medium for inter-valence-band lasers, Appl. Phys. Lett. 68 (1996) 3075.
[12] S. Komiyama, S. Kuroda, I. Hosaka, Y. Akasaka, N. Iizuka, Germanium lasers in the range from far-infrared to millimetre waves, Optical Quantum Electron. 23 (1991) S133–S134.